Brightness Temperatures of Snow Melting/Refreezing Cycles: Observations and Modeling Using a Multilayer Dense Medium Theory-Based Model

Marco Tedesco, *Member, IEEE*, Edward J. Kim, *Senior Member, IEEE*, Anthony W. England, *Fellow, IEEE*, Roger D. De Roo, *Member, IEEE*, and Janet P. Hardy

***Abstract*—The ability of electromagnetic models to accurately predict microwave emission of a snowpack is complicated by the need to account for, among other things, nonindependent scattering by closely packed snow grains, stratigraphic variations, and the occurrence of wet snow. A multilayer dense medium model can account for the first two effects. While microwave remote sensing is well known to be capable of binary wet/dry discrimination, the ability to model brightness as a function of wetness opens up the possibility of ultimately retrieving a percentage wetness value during such hydrologically significant melting conditions. In this paper, the first application of a multilayer dense medium radiative transfer theory (DMRT) model is proposed to simulate emission from both wet and dry snow during melting and refreezing cycles. Wet snow is modeled as a mixture of ice particles surrounded by a thin film of water embedded in an air background. Melting/refreezing cycles are studied by means of brightness temperatures at 6.7, 19, and 37 GHz recorded by the University of Michigan Truck-Mounted Radiometer System at the Local Scale Observation Site during the Cold Land Processes Experiment-1 in March 2003. Input parameters to the DMRT model are obtained from snow pit measurements carried out in conjunction with the microwave observations. The comparisons between simulated and measured brightness temperatures show that the electromagnetic model is able to reproduce the brightness temperatures with an average percentage error of 3% (~8 K) and a maximum relative percentage error of around 8% (~20 K).**

***Index Terms*—Cold Land Processes Experiment (CLPX), dense medium theory, microwave emission, microwave radiometry, remote sensing, snow, wet snow.**

I. Introduction

SNOW is a fundamental component of the Earth's water and energy cycles, acting as a major seasonal water reservoir as well as modulating the surface energy balance. Seasonal snow covers over 30% of the Earth's total land surface and more than half of the Northern Hemisphere land surface (~60%) in midwinter [1]. At high latitudes and altitudes, where snowfall is the dominant type of precipitation [2], melting snow is responsible for the majority of the total annual streamflow. Microwaves are sensitive to snow properties (e.g., phase of water, mean grain size, fractional volume, and snow depth), and many studies have been conducted on the relationships between snow parameters and electromagnetic signatures (e.g., [3] and [4]) as well as for retrieving snow parameters from satellite remotely sensed data (e.g., [5]–[7]). While visible and near-infrared sensors cannot see through clouds, microwave measurements are largely insensitive to weather conditions and do not require solar illumination. The microwave signal can also provide information on the internal properties of the snowpack, such as snow water equivalent, while visible and infrared sensors cannot.

Melting and refreezing cycles of snow generally occur near the beginning and the end of the snow-covered season. In dry snow, which can be represented for microwave modeling purposes as ice particles embedded in an air background, the volumetric scattering due to ice particles attenuates the microwave emission signal coming from the soil. In the case of wet snow, the snowpack can be modeled as a mixture of ice, liquid water, and air. Here, volumetric scattering is reduced while absorption increases. As the liquid water content (LWC) increases, the brightness temperature increases until a threshold value for the LWC is reached, after which an increase in the LWC is not followed by an increase in the brightness temperature. When snow refreezes, brightness decreases as a consequence of the decrease of LWC and temperature.

Analysis of the relationships between snowpack characteristics undergoing melting and refreezing cycles and the corresponding microwave brightness signatures can provide insight into the physical processes involved and improve retrievals of snow properties from spaceborne radiometric data. We also note that these insights will be critical for future snow-related radiance-based assimilation schemes. In this study, we use a multilayer electromagnetic model based on dense medium radiative transfer theory (DMRT) under the quasi-crystalline approximation with coherent potential (QCA-CP) [8], [9] to simulate the brightness temperatures recorded by the University of Michigan Truck-Mounted Radiometer System (TMRS) [10] of snow melting/refreezing cycles. The use of a multilayer model is crucial to account for the vertical distribution of snow parameters, such as wetness and mean grain size. It has

Manuscript received October 4, 2005; revised June 7, 2006.

M. Tedesco is with the University of Maryland, Baltimore County, Goddard Earth Sciences and Technology Center, NASA Goddard Space Flight Center, Greenbelt, MD 20771 USA (e-mail: mtedesco@umbc.edu).

E. J. Kim is with the Laboratory of Hydrospheric and Biospheric Sciences Laboratory, NASA Goddard Space Flight Center, Greenbelt, MD 20771 USA.

A. W. England and R. D. De Roo are with the University of Michigan, Ann Arbor, MI 48109 USA.

J. P. Hardy is with the Cold Regions Research and Engineering Laboratory, Hanover, NH 03755-1290 USA.

Digital Object Identifier 10.1109/TGRS.2006.881759

been demonstrated (e.g., [11]–[13]) that the use of a multilayer model improves the capabilities of the model to reproduce the observed brightness temperatures. Shih *et al.* [14] used a multilayer DMRT model to model the temporal signature of the millimeter-wave backscattering coefficient of snow undergoing melting and refreezing cycles with the support of the SNTHERM model, while Cagnati *et al.* [11] used an approach based on the combination of strong fluctuation theory and a hydrological model to simulate recorded brightness temperatures of melting/refreezing cycles in the Italian Alps. However, we found no examples in the literature of a multilayer DMRT model applied to the case of passive measurements (radiometry) of wet and dry snow conditions during melting/refreezing cycles. In this sense, the results reported in this study are based on a novel approach.

This paper is structured as follows. In Section II, the test site is described and the temperature profiles recorded by the meteorological station, and the snow pit data are presented and discussed. In Section III, the characteristics of the TMRS system are reported together with the temporal behavior of the recorded brightness temperatures. In Section IV, we describe the multilayer DMRT-based electromagnetic model. In Section V, we compare the modeled and observed brightness temperatures. We dedicate Section VI to the conclusions.

II. Measurement of Snow Properties

In this section, we describe the test site, the temporal trends of snow temperature profiles, and the values of the snow parameters collected from snow pits during the study period.

A. Local Scale Observation Site (LSOS)

The Cold Land Processes Experiment-1 (CPLX-1) design included multiple nested sites in Colorado, U.S. The largest study area was the large regional study area (LRSA, 375 km $\times$ 375 km), located in northern Colorado and southern Wyoming, U.S. The small regional study area (SRSA) was located in north-central Colorado (105°–107.5° W, 39.5°–41° N). Nested within the SRSA were the Fraser, North Park, and Rabbit Ears Meso-cell study areas (MSAs, 25 km $\times$ 25 km) used for airborne data collection. Nine intensive study areas (ISAs, 1 km $\times$ 1 km) were selected for intensive measurements. Within the Fraser ISA, near the Fraser Experimental Forest Headquarters Facility (39°50′49″ N, 105°54′40″ W), there was one LSOS (Fig. 1). Within the 100 m $\times$ 100 m LSOS, intensive ground observations of snow, soil, and vegetation were made in conjunction with stationary ground-based microwave remote sensing and micrometeorological observations during February and March of both 2002 and 2003. In total, four week-long intensive observation periods (IOPs) were conducted to observe dry (IOP1 and IOP3, February 2002 and 2003) and wet (IOP2 and IOP4, March 2002 and 2003) snow conditions. Meteorological measurements of snow and soil parameters were also recorded 24 h/day by the University of Michigan meteorological station. Snow pit measurements were carried out at two locations within 30 m of the area observed by the radiometer. In this study, we focus on the brightness temperatures recorded by the University of Michigan TMRS during IOP4 in conjunction with colocated meteorological and nivological measurements.

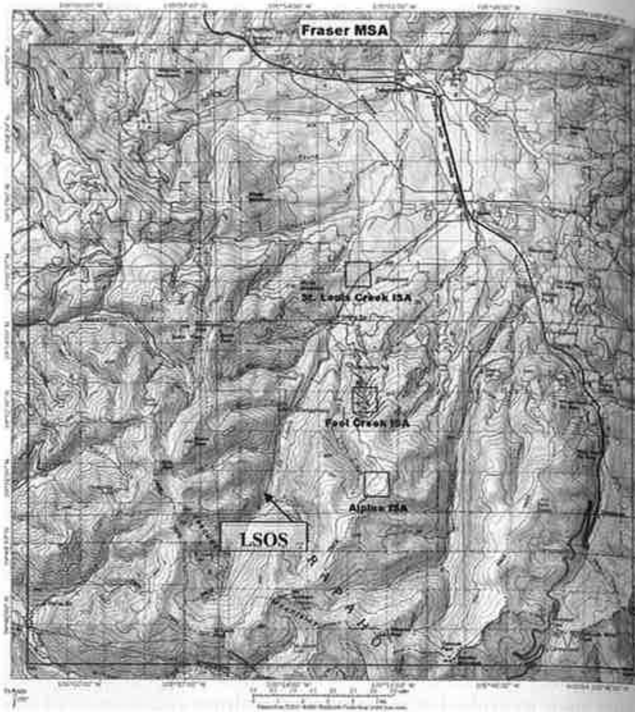

Fig. 1. Location of the LSOS inside the CLPX-1 Fraser 25 $\times$ 25 km MSA.

B. Air and Snow Temperature Profiles

Snow and air temperatures were recorded 24 h/day by the University of Michigan meteorological station using 14 probes at fixed heights above the ground surface (152.4, 143.0, 131.3, 119.6, 107.9, 96.2, 84.5, 72.8, 61.1, 49.4, 37.7, 26.0, 14.2, and 2.5 cm). The accuracy of the sensors was $< \pm$ 0.4 K, and the precision was $<$ 0.1 K (http://nsidc.org/data/docs/daac/nsidc0168_clpx_lsos_micromet/). As the thermometers were kept at fixed heights with respect to the ground surface, they measured either snow or air temperature, depending on the snow depth. Fig. 2(a) shows the temporal behavior of the temperatures collected between 154 and 84.5 cm above the ground surface. Fig. 2(b) plots the temporal behavior of the temperatures recorded between 84.5 and 61 cm, and Fig. 2(c) reports the temporal behavior of the temperatures recorded between 48.5 cm and the ground surface. The probes between 154 and 72.8 cm always measured air temperature. The probes between 72.8 and 61.1 cm were sometimes covered by snow during IOP4, depending on the snow depth, and those between 61.1 cm and the ground surface were always covered by snow. Recorded data show that during the period between 00:00 (local time) March 25, 2003 and 12:00 March 27, 2003 (corresponding to 60 h from the reference time 00:00 March 25, 2003), the temperature of the upper part of the snow oscillated around 0 °C, with the air temperature ranging between -15 °C and $+6$ °C [Fig. 2(b)]. The temperature of the bottom part of the snowpack was always slightly higher than zero (0.4 °C $\pm$ 0.2 °C) and stable [Fig. 2(c)], suggesting that the bottom part of the snowpack was wet for the entire IOP4. On the other hand, the upper part of the snowpack was subject to melting and refreezing cycles. In the period between March 27, 2003 (72 h from the reference time) and the end of IOP4, a change in the trend of temperatures recorded at 49.5 and 37.7 cm is noticeable. This can be attributed to the rapid decrease of air

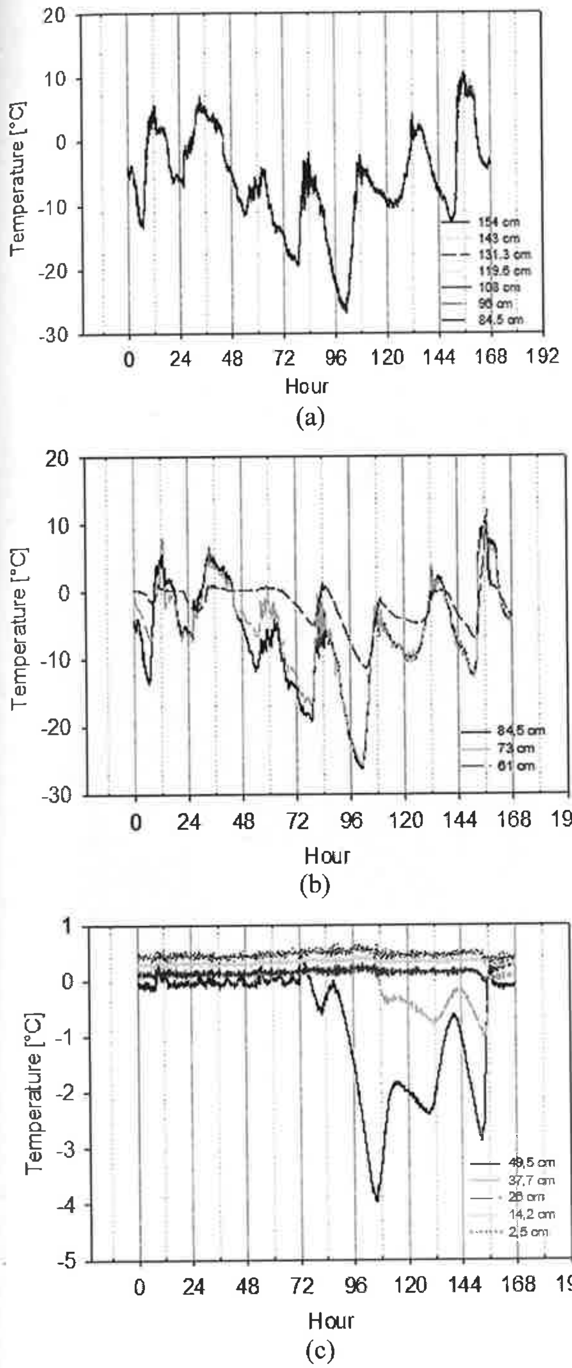

Fig. 2. Temporal behavior of temperatures at different heights above ground level recorded by the University of Michigan meteorological station during the IOP4. The zero reference time is March 25, 00 : 00 local. (a) The probes between 154 and 84.5 cm measured air temperature for the entire IOP4. (b) The probes between 72.8 and 61.1 cm were sometimes covered by snow, depending on the snow depth. (c) The probes between 61.1 cm and the ground surface were always covered by snow.

temperature and to the observed presence of new snow at the top of the snowpack.

C. *Snow Pit Measurements*

During IOP4, values of snow depth, density, temperature, wetness, and mean grain size were collected along the vertical profile of the snowpack at different locations within the LSOS [15]. Two of these locations (denoted as #3 and #4 within the framework of the CLPX-1, http://www.nohrsc.nws.gov/~cline/clpx.html) were close to the snow monitored by the meteorological station and observed by the TMRS. Location #3 was located 20 m in front of the field of view (FOV) of the TMRS, and location #4 was 30 m to the rear. The snow pit data used for our study were collected from snow pit location #3 on March 26, 2003 at 10 : 00 (3A), March 28, 2003 at 16 : 50 (3B), and March 30, 2003 at 16 : 00 (3C), and from snow pit location #4 on March 25, 2003 at 10 : 50 (4A), March 27, 2003 at 11 : 45 (4B), and March 29, 2003 at 14 : 30 (4C). The values of snow parameters averaged along the vertical profile are reported in Table I. These values are used as inputs to the electromagnetic model in Section IV to simulate the observed brightness temperatures. The number of layers into which the snowpack was divided was initially set to $n = 3$. This value was suggested by the number of distinctive layers identified considering the wetness and mean grain size distributions. However, because of the high wetness values of the layer in the middle of the snowpack (second layer), we found, in practice, that the number of model layers could be reduced to $n = 2$. Indeed, the penetration depth in wet snow at the frequencies and wetness values of interest is of the order of a few centimeters, i.e., less than the thickness of the middle layer. Fig. 3 shows the daily measured snow wetness profiles, with dry snow represented by white, snow with wetness between 0% and 0.5% shown by light gray, snow with wetness between 0.5% and 1% shown by medium gray, snow with wetness between 1% and 1.5% shown by dark gray, and finally, snow with wetness higher than 1.5% shown by black. The thicknesses of the two model layers changed depending on the snow wetness profile: the first (upper) layer represented a part of the snowpack subject to melting and refreezing, whereas the second (bottom) layer represented a layer that was always wet during the entire IOP4. Fig. 4 shows a photograph of the snow pit where measurements were performed on March 29, 2003. In the picture, the different layers are distinctly observable. The measured profiles of snow wetness are consistent with the bottom part of the snowpack being wet for the entire IOP4, as indicated by the temperature probe data. With regard to the upper part of the snowpack, data collected on March 25, 2003 show that a dry snow layer was overlying two layers of wet snow of different wetness that, in turn, were overlying another layer of dry snow over wet snow (Fig. 3). On March 26, 2003, the upper part of the snowpack was also wet, whereas on March 27, 2003, it was almost dry ($w = 0.06\%$). On March 28 and March 29, 2003, the upper part of the snowpack was again dry. On March 30, 2003, another dry snow layer was present between the wet snow layers.

III. Microwave Radiometric System and Data

In this section, we examine the microwave signatures of melting and refreezing cycles of the LSOS snowpack recorded by the University of Michigan TMRS during IOP4.

Radiometric data at 6.7 (horizontal polarization), 19, and 37 GHz (vertical and horizontal polarizations) were recorded 24 h/day with an incidence angle of 53°. The 19- and 37-GHz systems had beamwidths of 10° each, while the 6.7-GHz system had a beamwidth of 22°. The antennas were mounted on the end of a 10-m telescoping boom with an elevation positioner at the

TABLE I
SNOW PARAMETERS OF SNOW LAYER PARAMETERS DERIVED FROM SNOW PIT DATA AND ALSO GIVEN AS INPUTS TO THE ELECTROMAGNETIC MODEL TO SIMULATE THE TMRS RECORDED BRIGHTNESS TEMPERATURES

Date (Snow pit)	Thickness [m]		Density [kg/m³]		Temperature [K]		Wetness [%]	
	Upper	Lower	Upper	Lower	Upper	Lower	Upper	Lower
03/25/2003 (4A)	0.15	0.40	230	250	272	273.15	0	0.5
03/26/2003 (3A)	0.1	0.71	195	306	273.15	273.15	0.3	0.7
03/27/2003 (4B)	0.35	0.30	190	277	272.5	273.15	0.06	1
03/28/2003 (3C)	0.4	0.45	223	331	269.2	273.15	0	0.2
03/29/2003 (4C)	0.20	0.4	225	294	270	273.15	0	0.6
03/30/2003 (3C)	0.1	0.77	214	301	273.15	273.15	1.3	1.5

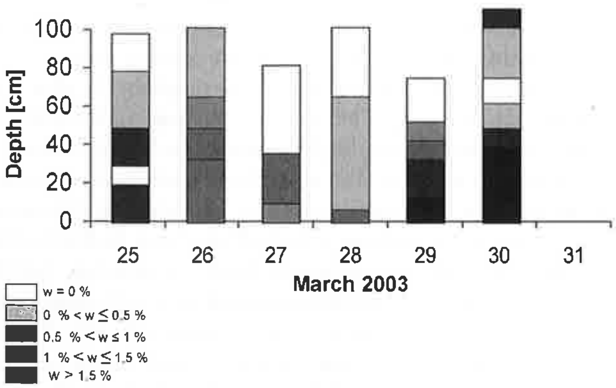

Fig. 3. Snow wetness (w) profiles collected at snow pits #3 (March 26, 28, and 30, 2003) and #4 (March 25, 27, and 29, 2003). White: dry snow. Light gray: $0\% < w \leq 0.5\%$. Medium gray: $0.5\% < w \leq 1\%$. Dark gray: $1\% < w \leq 1.5\%$. Black: $w > 1.5\%$.

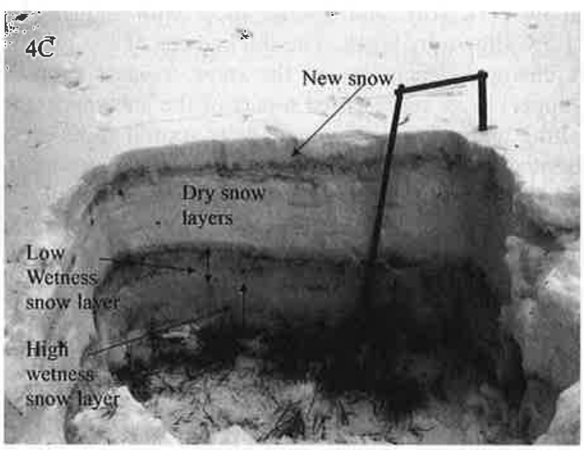

Fig. 4. Photograph of snow pit #4 on March 29, 2003. The different types of observed layers are indicated. The total snow depth was 60 cm.

end of the boom (Fig. 5). For all the radiometers, the precision was ±0.5 K. The 6.7-, 19-, and 37-GHz brightness temperatures were accurate to ±3 K. The 6.7-GHz V-pol data could not be calibrated and, therefore, will not be used in this study. During a 4-s interval, each radiometer antenna monitored a reference brightness both before and immediately after the target observation. Data were discarded if the references differed by more than 3 K, which was considered to be an indication of unstable electronics or thermal control of the electronics. Small changes in the physical temperature of the amplifiers can produce changes in the radiometer output that are indistinguishable from brightness changes. Therefore, data were flagged and discarded if the amplifier physical temperature changed or differed from the calibration temperature by more than 1 °C.

Fig. 5. Photograph of the University of Michigan TMRS operating at the LSOS during the IOP4 of the CLPX-1.

The temporal behaviors of the brightness temperatures recorded at 6.7-GHz horizontal polarization (dark gray), 19 GHz (light gray), and 37 GHz (black) by the TMRS are plotted in Fig. 6. Air and surface snow temperatures, represented by the temperatures recorded at 61.1 and 72.8 cm above the ground by the meteorological station, are also reported. Two complete melting–refreezing cycles occurred within the first 36 h of the IOP4 (the zero reference time is local 00:00 March 25, 2003). No melting cycle occurred in the period between March 26 at 12:00 and March 29 at 10:00 (60 and 130 h in Fig. 6) when the recorded brightness temperatures decrease, reaching a minimum on March 27 at 4:00 (100 h). This is due to both the decrease of the snow temperature (Fig. 2) and to the increase of the mean particle size, as confirmed by snow pit measurements. After this period, new melting–refreezing cycles were observed until the end of the IOP4. The observed behavior of the brightness temperatures can be explained considering that for dry snow, volumetric scattering is dominant versus absorption, and to a first approximation, the brightness temperature can be modeled as the brightness temperature of the soil reduced by the scattering of dry snow particles plus the emission from the snow itself. When snow melts, the imaginary part of its permittivity increases as does the absorption coefficient, and the radiation emitted by the soil is masked by snow absorption. For wet snow, the main contribution to

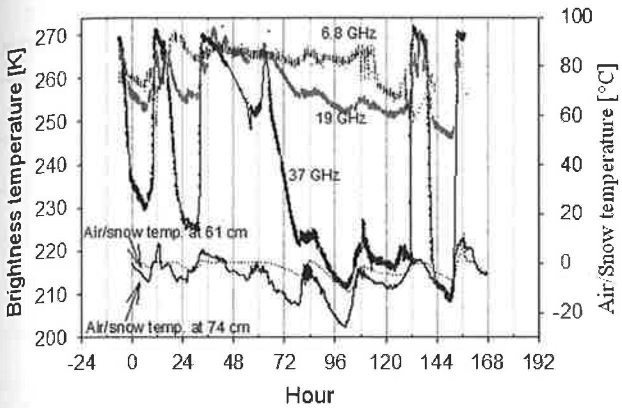

Fig. 6. Brightness temperature signatures at 6.7-GHz (dark gray) horizontal polarization and at 19-GHz (light gray) and 37-GHz (black) vertical polarization measured by the TMRS. Air/snow temperatures recorded at 61 cm (dots) and 74 cm (solid) are also plotted. Reference time is March 25, 2003 00 : 00 local.

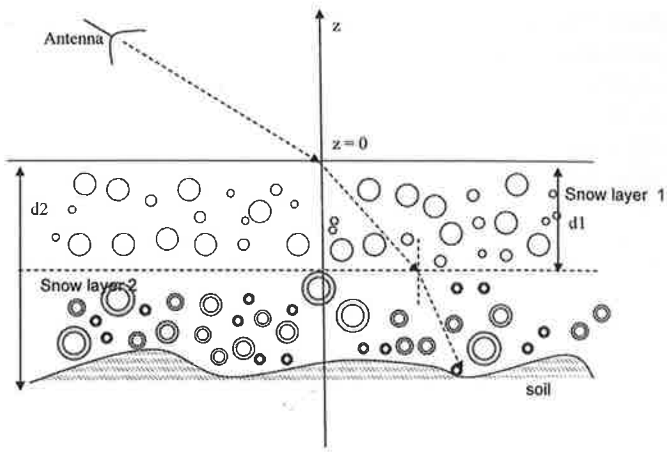

Fig. 7. Representation of the snowpack used in the electromagnetic model in the case of two layers ($n = 2$). The upper layer is dry, and the bottom layer is wet. Ice particles in snow are modeled as spherical particles. Liquid water is modeled as a thin film surrounding ice particles.

the recorded brightness temperature is from the snowpack. The brightness temperatures increase as the wetness increases until a saturation value of brightness temperature is reached, after which the brightness temperatures remain constant as the wetness increases. During the refreezing, the brightness temperatures decrease as the LWC and temperature in the snowpack decrease. At 37 GHz, the changes in brightness temperatures due to the melting–refreezing cycles are stronger than those at 19 GHz. This can be explained by considering that the higher frequency is more sensitive to the changes of the snowpack properties (i.e., temperature, wetness, grain size) near the surface, where the melting or refreezing was occurring. As expected, at 6.7 GHz, the sensitivity to the melting/refreezing cycles is very weak because of the large penetration depth.

IV. Electromagnetic Model

The brightness temperatures collected by the TMRS were simulated by a multilayer electromagnetic model based on the DMRT [8], [9] with the inputs to the model derived from the data collected at the snow pits and from the meteorological station.

In a dense medium such as snow, the assumption of independent scattering is no longer valid, and the scattering of correlated scatterers must be considered. In the DMRT, this is done by considering pair distribution functions of the particle positions, and the medium is modeled as spherical scatterers embedded in a background medium with permittivity ε_b (e.g., air). In the model, the snowpack is divided into n layers, and each layer is treated as a slab of distributed spherical particles with the following inputs: radius a, thickness d, wetness w (expressed as a percentage by volume), total fractional volume f (given by the density of snow divided by the density of ice: $\rho_{\text{snow}}/\rho_{\text{ice}}$), and permittivity ε_{ws} (which is not a direct input but it is derived from other inputs as explained in the following) (Fig. 7). For each layer, the total fractional volume is expressed by $f = f_{\text{ice}} + w/100$, where f_{ice} represents the fractional volume occupied by the ice particles, and w is the snow wetness. The ice permittivity is computed according to [16]. The extinction coefficient and the albedo are computed for each of the n layers according to the DMRT [8]. Introducing K_0 satisfies the relation [8]

$$K_0^2 = k^2 + \frac{f\left(k_s^2 - k^2\right)}{1 + \frac{k_s^2 - k^2}{3K_0^2}(1-f)} \tag{1}$$

where k and k_s are, respectively, the wavenumbers of the background and the particles, and f is the fractional volume occupied by particles. Physically, K_0 indicates the propagation constant of coherent waves in a medium where the scattering effect can be ignored. Mathematically, K_0 is regarded as the zeroth order solution of the effective wavenumber K that can be obtained as [8]

$$\begin{aligned} K^2 &\cong K'^2 + 2iK'K'' \\ &= k^2 + \frac{f\left(k_s^2 - k^2\right)}{1 + \frac{k_s^2 - k^2}{3K_0^2}(1-f)} \\ &\quad \cdot \left\{ 1 + i\frac{2}{9}\frac{K_0 a^3\left(k_s^2 - k^2\right)}{1 + \frac{k_s^2 - k^2}{3K_0^2}(1-f)}\frac{(1-f)^4}{(1+2f)^2} \right\}. \end{aligned} \tag{2}$$

Subsequently, the extinction rate k_e and albedo ω are obtained as

$$k_e = 2\mathrm{Im}(K) \tag{3}$$

$$\omega = \frac{2}{9}\frac{a^3 f}{k_e}\left|\frac{k_s^2 - k^2}{1 + \frac{k_s^2 - k^2}{3K_0^2}(1-f)}\right|^2 \frac{(1-f)^4}{(1+2f)^2}. \tag{4}$$

We model wet snow as ice particles surrounded by a thin film of water. The effective dielectric constant of ice spheres with a water coating is given by [17]

$$\frac{\varepsilon_{ws} - \varepsilon_0}{\varepsilon_{ws} + \varepsilon_0} = \frac{(\varepsilon_w - \varepsilon_0)(\varepsilon_i + \varepsilon_w) + S(\varepsilon_i - \varepsilon_w)(\varepsilon_0 + 2\varepsilon_w)}{(\varepsilon_w + 2\varepsilon_0)(\varepsilon_i + 2\varepsilon_w) + 2S(\varepsilon_w - \varepsilon_0)(\varepsilon_i - \varepsilon_w)} \tag{5}$$

where ε_{ws} is the effective permittivity of the water-coated spherical ice particles, ε_w is the water permittivity, ε_i is the ice permittivity, and $S = a_{\text{ice}}/a_{\text{water}}$, where a_{ice} and a_{water} are the inner (only the ice particles) and outer (ice particles plus water film) radii of the modeled spheres. The inner and outer radii may be related, and the parameter S is given by $S = (f_{\text{ice}}/f_{\text{tot}})^{1/3}$ [8]. The final DMRT equations assume a form resembling the conventional radiative transfer theory and can be solved by using discrete ordinates, Gaussian quadrature, or the eigenvalues and eigenvectors methods [8]. The unknown coefficients used to derive the particular solution from the eigenvector solutions are determined by imposing the boundary conditions. For example, in the case of two layers ($n = 2$), we have (e.g., [8]) $\overline{I}_1(\pi - \theta_1, 0) = \overline{\overline{R}}_{10}(\theta_1) \cdot \overline{I}_1(\theta_1, 0)$ at $z = 0$, $\overline{I}_1(\theta_1, -d1) = \overline{\overline{R}}_{12}(\theta_1) \cdot \overline{I}_1(\pi - \theta_1, -d1) + \overline{\overline{T}}_{21}(\theta_1) \cdot \overline{I}_2(\theta_2, -d1)$ and $\overline{I}_2(\pi - \theta_2, -d1) = \overline{\overline{R}}_{21}(\theta_2) \cdot \overline{I}_2(\theta_2, -d1) + \overline{\overline{T}}_{12}(\theta_2) \cdot \overline{I}_1(\pi - \theta_1, -d1)$ at $z = -d1$, where $d1$ is the thickness of the first layer, and $\overline{I}_2(\theta_2, -d2) = \overline{\overline{R}}_{2\text{soil}}(\theta_2) \cdot \overline{I}_2(\pi - \theta_2, -d2) + \overline{\overline{T}}_{\text{soil}2}(\theta_2) \cdot C \cdot T_{\text{soil}}$ at $z = -d2$ (snow/soil interface) with θ_i ($i = 1, 2$) obeying Snell's law. In the model, we account for the roughness at the soil/snow interface by means of the so-called Q/H model [18], whose parameters Q and H were found through a fitting procedure during measurements carried out in dry snow conditions. The parameter Q describes the energy emitted in orthogonal polarizations due to surface roughness effects, and H is a measure of the effect of surface roughness to increase surface emissivity. The values for Q and H used in this study are, respectively, $Q = 0.35$ and $H = 0.4$. However, in the cases under study, the bottom of the snowpack was always wet, and therefore, the effect of roughness at the snow/soil interface plays an insignificant role in the calculation of the brightness temperatures. The roughness at the snow/air interface and the snow/snow interlayer interface is set to zero (smooth surfaces). The ground permittivity and temperature were fixed, respectively, at $\varepsilon_{\text{soil}} = 3.5 + i0.1$ and $T_{\text{soil}} = 273.15$ K. Table II summarizes the list of inputs and symbols of the quantities used in the electromagnetic model.

TABLE II
LIST OF INPUTS AND SYMBOLS USED IN THE ELECTROMAGNETIC MODEL

Direct input and symbols	
d_i	**Depth of bottom part of the ith layer**
a_i	Radius of ice particles
f_i	Total fractional volume
w_i	Wetness
T_i	Snow temperature
T_{soil}	Soil temperature
Q	Q Parameter in the Q/H model
H	H parameter in the Q/H model
ε_{soil}	Soil permittivity
Inputs and symbols derived	
$\overline{\overline{R}}_{ij}$	ith – jth layers reflectivity
$\overline{\overline{R}}_{n-soil}$	nth layer – soil reflectivity
$\overline{\overline{T}}_{n-soil}$	nth layer – soil transmissivity
$\overline{I}_i$	Stokes vector
C	$= B\varepsilon'/(\lambda^2\varepsilon_0)$
ε_i	Ice permittivity
ε_{ws}	Snow permittivity
k_e	Extinction coefficient
ω	Albedo

The sensitivity of the DMRT in the case of a single layer of dry snow has been investigated, and the results are reported in the literature (e.g., [3], [4], [8], [9], and [12]). In the following, we report an example of the sensitivity analysis of the multilayer DMRT-based model with respect to the snow wetness. We simulate the brightness temperatures of a snowpack with two layers and consider two different scenarios. In the first scenario, we consider a configuration where the bottom layer of the snowpack is dry and the upper layer is subject to melting. The following input parameters are used: $d_1 = 0.3$ m, $d_2 = 0.8$ m, w_1 ranging between 0% and 1%, $w_2 = 0\%$, $T_1 = 273.15$ K, $T_2 = 272$ K, $a_1 = a_2 = 0.5$ mm, $f_1 = f_2 = 0.3$, $\varepsilon_{\text{ground}} = 3.5 + i * 0.1$. Fig. 8 shows the simulated brightness temperatures at (a) 19 and (b) 37 GHz (vertical polarization) as a function of the wetness (of the upper layer). In the figure, we also plot the contributions from the different layers to the total brightness. Note that the left axes refer to the different contributions from the layers and soil, where the right axes refer to the total brightness temperature. As expected, the total brightness temperature increases as the wetness increases, saturating when the value of wetness exceeds 1%. Beyond this, a further increase in the wetness does not further increase the brightness temperature. As the wetness of the upper layer increases, the contribution from the upper layer (wet layer) to the total brightness temperature increases, while the contribution from the soil and dry snow layer is reduced. This trend can be explained considering that absorption within the wet (upper) snow layer increases as the wetness increases so that the radiation coming from the underlying snow layer and soil is masked while emission from the upper layer increases. In the second scenario, we consider a snowpack where the upper layer is dry and the bottom one is subject to melting. The parameters used in this case are $d_1 = 0.8$ m, $d_2 = 0.3$ m, $w_1 = 0\%$, w_2 ranging between 0% and 1%, $T_1 = 272$ K, $T_2 = 273.15$ K, $a_2 = a_1 = 0.5$ mm, $f_1 = f_2 = 0.3$, $\varepsilon_{\text{ground}} = 3.5 + i * 0.1$. Similar to Fig. 8, Fig. 9 displays the simulated brightness temperatures at (a) 19 and (b) 37 GHz (vertical polarization) as a function of the wetness (of the bottom layer) together with the contributions from the different layers to the total brightness temperature. We observe that the contribution due to soil decreases as the wetness of

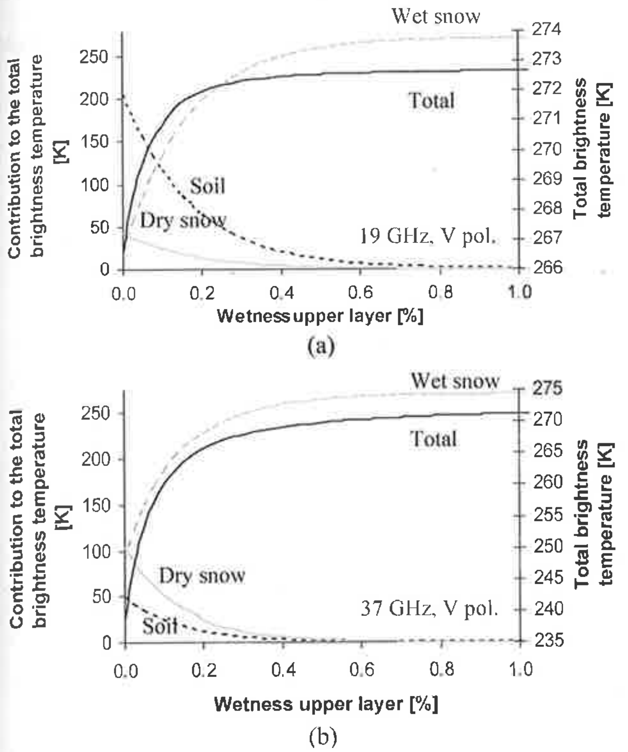

Fig. 8. Simulated total brightness temperatures (right axes) at (a) 19 GHz and (b) 37 GHz (vertical polarization) as a function of wetness of the upper layer. All remaining snow parameters are kept fixed as follows: $d_1 = 0.3$ m, $d_2 = 0.8$ m, w_1 ranging between 0% and 1%, $w_2 = 0\%$, $T_1 = 273.15$ K, $T_2 = 272$ K, $a_2 = a_1 = 0.5$ mm, $f_1 = f_2 = 0.3$, and $\varepsilon_{\text{ground}} = 3.5 + i * 0.1$. The contributions (left axes) from the different layers to the total brightness temperature are also plotted.

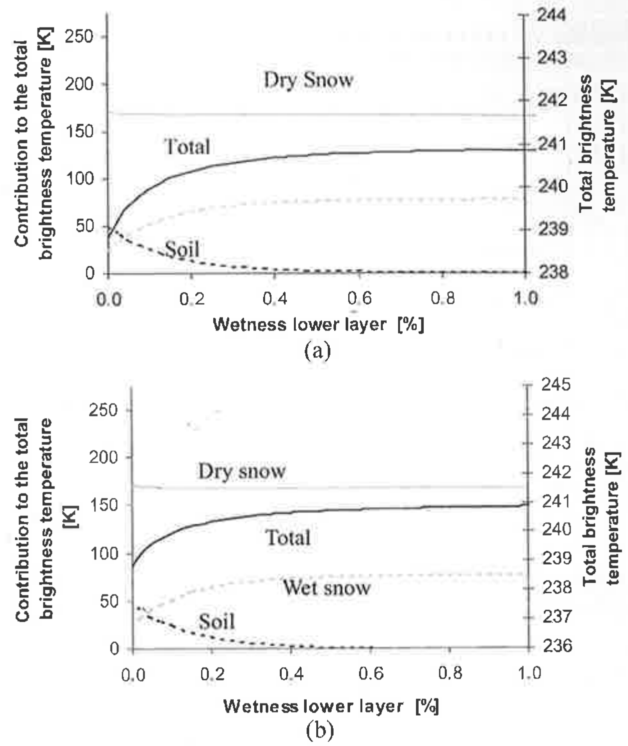

Fig. 9. Simulated total brightness temperatures (right axes) at (a) 19 GHz and (b) 37 GHz (vertical polarization) as a function of wetness of the bottom layer. All remaining snow parameters are kept fixed as follows: $d_1 = 0.8$ m, $d_2 = 0.3$ m, $w_1 = 0\%$, w_2 ranging between 0% and 1%, $T_1 = 272$ K, $T_2 = 273.15$ K, $a_2 = a_1 = 0.5$ mm, $f_1 = f_2 = 0.3$, and $\varepsilon_{\text{ground}} = 3.5 + i * 0.1$. The contributions (left axes) from the different layers to the total brightness temperature are also plotted.

the bottom layer increases, because of the increased absorption. At the same time, the contribution of the bottom layer of the snowpack increases as the LWC (and the emissivity) of the layer increases.

V. Modeling of Experimental Data: Results and Discussion

In the following, brightness temperatures simulated by means of the multilayer DMRT-based model are compared with the brightness temperatures observed by the TMRS. To obtain the inputs to the electromagnetic model, the values of the snow parameters measured at the snow pits are vertically averaged. The averaged snow parameters are reported in Table I. The number of significant layers was fixed to $n = 2$. As explained in Section II, by comparing results for $n = 2$ and $n = 3$, we found that the case with $n = 3$ did not yield significantly better results when simulating the IOP4 brightness signatures. Indeed, the difference between the brightness temperatures simulated in the case with $n = 2$ and $n = 3$ was on the order of a few hundredths of kelvin at 6.8 GHz and even lower for higher frequencies.

When the measured wetness values of the upper part of the snowpack exceeded 1%, only the upper layer was modeled. This is because wetness measurements were carried out every 10 cm along the vertical profile, and the penetration depth at the frequencies of interest for values of wetness higher than 1% is less than 10 cm (e.g., [12] and [19]).

The mean particle size is the parameter to which brightness temperatures show strong sensitivity, especially at 37 GHz. The profiles of the three classes of particle size (Small, Medium, and Large) along both short and long particle axes were collected at the snow pit locations. To investigate the sensitivity of the brightness temperatures to the three classes, three different values of mean particle size were considered as inputs to the electromagnetic model. In case A, the value of the mean particle size is derived by averaging the values of measured grain size of all three classes. In case B, we used only the values of the Medium and Large classes. And in case C, we used only the values of the Large class. Table III shows the averaged particle size values for the different dates.

In case A, the electromagnetic model predicts brightness temperature values higher than the measured values. Table IV reports average values of the ratio $T_{\text{meas}}/T_{\text{sim}}$ (expressed in percentage) and of the relative percentage error between measured and simulated brightness temperatures ($\text{abs}(T_{\text{meas}} - T_{\text{sim}})/T_{\text{meas}})$) for the three classes of grain size. We observe that in the case under consideration (Small grain size), the average values of the ratio tend to be smaller than 100 (in percentage), meaning that the model tends to overestimate measured brightness temperatures.

The best results were obtained with the values of mean grain size used in case B. From Table IV, we can observe that the average values of the ratio do not show a particular trend. We also observe that the average values of the relative percentage error are smaller than the ones obtained in case A (Small grain

TABLE III
AVERAGE VALUES OF MEAN PARTICLE SIZE FOR THE MODEL LAYERS OBTAINED BY AVERAGING THE VALUES OF THE SMALL, MEDIUM, AND LARGE CLASSES (LEFT), ONLY THE VALUES OF THE MEDIUM AND LARGE (CENTER), AND ONLY THE VALUES OF THE LARGE CLASS (RIGHT)

Date (Snow pit)	Avg. using Small, Medium and Large		Avg. using Medium and Large		Avg. using Large	
	Upper layer	Lower layer	Upper layer	Lower layer	Upper layer	Lower layer
03/25/2003 (4A)	0.41	0.58	0.5	0.69	0.61	0.9
03/26/2003 (3A)	0.55	1.23	0.65	1.6	0.8	2.15
03/27/2003 (4B)	0.56	1.17	0.75	1.4	0.9	1.8
03/28/2003 (3C)	0.31	1.35	0.42	1.65	0.56	2.05
03/29/2003 (4C)	0.59	1.25	0.7	1.68	0.9	2.1
03/30/2003 (3C)	0.28	1.8	0.37	2.25	0.5	2.7

TABLE IV
AVERAGE VALUES OF THE RATIO T_{meas}/T_{sim} (EXPRESSED IN PERCENTAGE) AND OF THE RELATIVE PERCENTAGE ERROR BETWEEN MEASURED AND SIMULATED BRIGHTNESS TEMPERATURES ($\mathrm{abs}(T_{meas} - T_{sim})/T_{meas}$)) FOR THE THREE CLASSES OF SMALL, MEDIUM, AND LARGE GRAIN SIZES

	Small		Medium		Large	
	Average value of (T_{meas}/T_{sim}) [%]	Average relative percentage error [%]	Average value of (T_{meas}/T_{sim}) [%]	Average relative percentage error [%]	Average value of (T_{meas}/T_{sim}) [%]	Average relative percentage error [%]
6.7 H	100.66	1.79	101.38	1.73	101.45	1.69
19 V	98.10	1.95	102.53	2.45	99.08	0.93
19 H	99.83	6.52	99.46	3.30	100.92	6.06
37 V	94.28	7.49	102.49	2.35	104.49	7.04
37 H	97.32	8.43	100.30	1.09	122.82	18.34

size). Fig. 10 shows the comparison between measured and modeled brightness temperatures at (a) 6.7 GHz, (b) 19 GHz, and (c) 37 GHz using the values of mean particle size derived in case B. In the figure, squares represent measured brightness temperatures, and circles represent simulated brightnesses by means of the multilayer model. Filled symbols indicate vertical polarization, and open symbols indicate horizontal polarization. The error bars associated with the simulated quantities represent the range of values of the brightness temperatures when the mean grain sizes are allowed to range ± 0.1 mm around the original value. The value of 0.1 mm is selected because it represents the resolution of the grain size measurements (e.g., the grain size dimension is rounded to the nearest 0.1 mm).

Fig. 11 shows the relative percentage error for each date at 6.7 GHz (horizontal polarization) and at 19 and 37 GHz (both vertical and horizontal polarizations). The maximum error is 7.73% (19.8 K), occurring for the 37-GHz channel, horizontal polarization, on March 26, 2003. We note other cases when the absolute error is relatively high. For example, on March 27, 2003, the error at 19-GHz horizontal polarization is 4.67% ($\sim$12 K); on March 29, 2003, the error at 37-GHz vertical polarization is 6.34% ($\sim$14 K), while it is less than 1% ($\sim$2.2 K) for the other polarizations; on March 28, 2003, the percentage errors for 19-GHz horizontal polarization and 37-GHz vertical polarization are, respectively, 5.89% and 5.63% ($\sim$12 K). All remaining cases show a relative percentage error of less than or equal to 3% ($\sim$6–8 K).

Results show that, in general, the simulated brightness temperatures are lower than measured ones with the exception of the 19-GHz vertical polarization on March 25 and March 29, 2003, and the 37-GHz vertical polarization on March 28 and 29, 2003. There are several factors that can contribute to this behavior. First, overestimating the values of the mean particle size would lead to underestimated brightness temperatures. In the case under analysis (case B), only the Medium and Large class particles are used to derive the input to the electromagnetic model. The net effect of the Small class particles may have been significant. However, exploring this would have required more specific measurements (e.g., the full particle size distribution) not available from CLPX-1. A second factor is related to the choice of the modeling of wetness in snow. For simplicity, in our model, all ice particles are considered to be surrounded by a thin film of water. In reality, some water can be present in the form of free particles with different shapes, and the shape of these water particles influences the values of wet snow permittivity (e.g., [20]). Modeling and computing the fraction of liquid water coating ice particles are difficult tasks, and no general rule has been found in the literature. For this reason, we chose to approximate all ice particles as coated by a film of water.

In case C, the model tends to underestimate the experimental data, especially at higher frequency. The values of the average percentage error are generally greater than those obtained in case B (Medium class) and comparable to those obtained in case A.

VI. CONCLUSION

Microwave brightness temperatures of snow melting/refreezing cycles were recorded in Colorado at 6.7, 19, and 37 GHz by the University of Michigan Tower-mounted

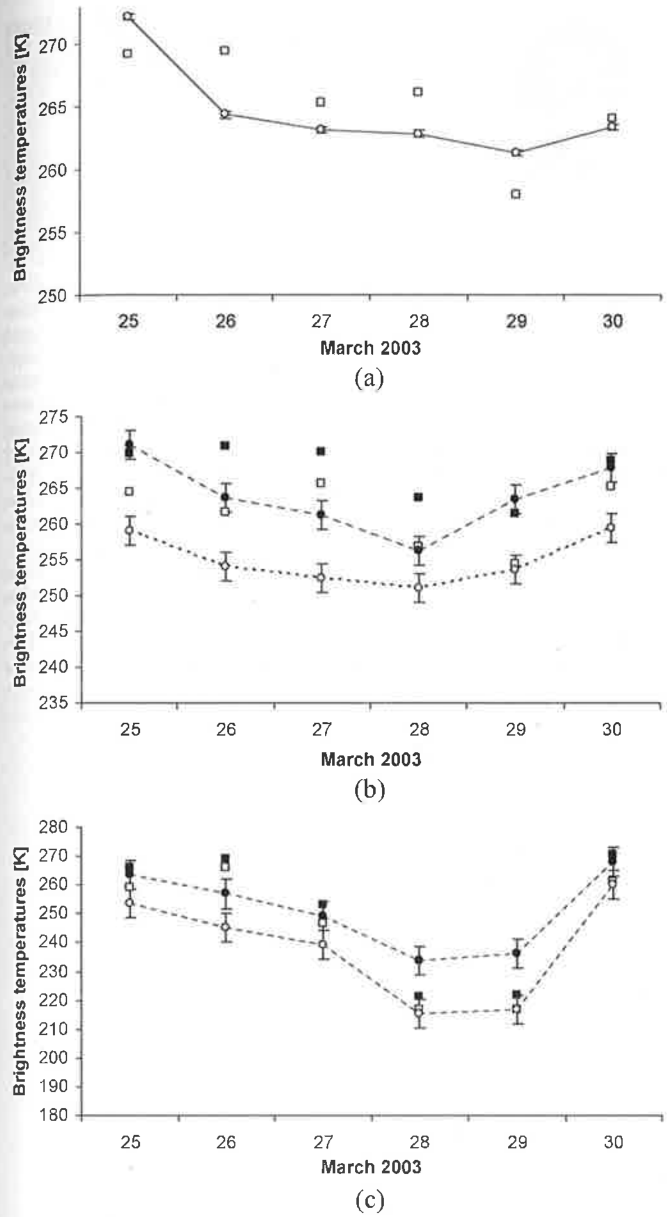

Fig. 10. Comparison between measured (squares) and DMRT simulated brightness temperatures at (a) 6.7 GHz, (b) 19 GHz, and (c) 37 GHz in the case of multiple layers (circles). All input parameters are derived from snow pit measurements. Filled symbols indicate vertical polarization, whereas open symbols indicate horizontal polarization. The error bars associated with the simulated quantities represent the range of values of the brightness temperatures when the mean grain sizes are allowed to range ±0.1 mm around the original value.

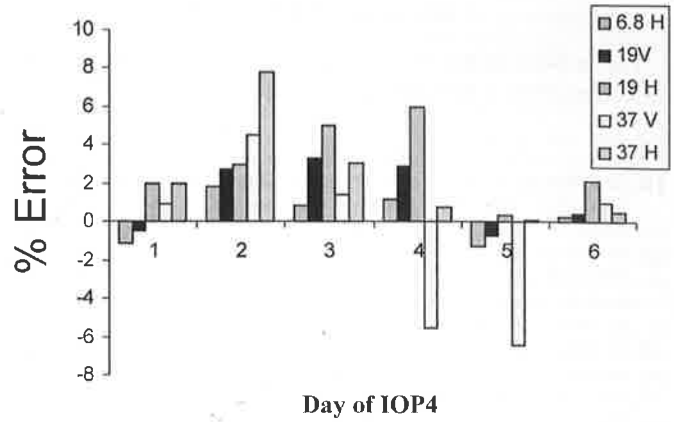

Fig. 11. Percentage error between measured and simulated brightness temperatures at 6.7 GHz (horizontal polarization) and at 19 and 37 GHz (vertical and horizontal polarizations).

Radiometer System (TMRS) on March 2004 within the framework of the Cold Land Processes Experiment-1. Snow conditions and meteorological data were also collected. Collected data confirm that the 37-GHz channel is the most sensitive to melting and refreezing cycles. Sensitivity decreases as frequency decreases. The greater penetration depth at low frequencies is the main cause of the reduced sensitivity.

A novel approach based on a multilayer electromagnetic model using dense medium theory was used to simulate the observed brightness temperatures with the inputs derived from snow pit data and temperature profiles. In the model, wet snow was treated as a mixture of ice particles surrounded by a film of water embedded in a background of air. Three different classes of mean grain size were measured (Small, Medium and Large classes). As no information on the grain size distribution was available, different combinations of the values of the three classes were explored as inputs to the model (e.g., combination of Small, Medium, and Large, combination of Medium and Large, and only Large particles).

Simulated brightness temperatures were compared with those acquired by the TMRS. Results show that the model was able to reproduce measured brightness temperatures with good accuracy although the choice of particle size class used to derive inputs to the model strongly influences the model's performance. When all three classes of particle size were considered, the model overestimated the brightness temperatures (maximum percentage error ~15%). This suggests that the derived mean particle size was too small. When only the Large particle sizes were used, the model strongly underestimated the brightness temperatures with a maximum percentage error of ~28%. This suggests that the derived mean particle size was too large. The best match between modeled and measured brightness temperatures was achieved using values from the Medium and Large classes to derive the mean grain size as input to the model. In this case, the maximum percentage error equals 7.73% (19.8 K) for 37-GHz vertical polarization, and the average percentage error for all frequencies and dates is 3% (~8 K). However, with this choice, we observed that the model tended to underestimate the brightness temperatures. Disregarding the contribution of the Small class particles may be the cause of the observed underestimation. Collecting information on the distribution of the grain size (i.e., how many particles belonging to each of the three classes) would greatly improve our capabilities to resolve the differences between simulated and observed brightness temperatures.

The capabilities of the electromagnetic model to reproduce the observed brightness temperatures might also be improved by modifying the modeling of wetness itself. In our model, all ice particles are assumed to be surrounded by a thin film of water. This is not always true in nature, but our choice was dictated by the fact that the relationship between wetness and fractional volume of free water in snow is practically unknown. Experiments aimed at describing such relationship might provide useful information for future studies.

ACKNOWLEDGMENT

The authors would like to thank all people involved in the collection of the CLPX data.

REFERENCES

[1] D. Robinson, K. Dewey, and R. Heim, "Global snow cover monitoring: An update," *Bull. Amer. Meteorol. Soc.*, vol. 74, no. 9, pp. 1689–1696, 1993.

[2] M. Serreze, M. Clark, R. Armstrong, D. McGinnis, and R. Pulwarty, "Characteristics of the western United States snowpack from snowpack telemetry (SNOTEL) data," *Water Resour. Res.*, vol. 35, no. 7, pp. 2145–2160, 2000.

[3] G. Macelloni, S. Paloscia, P. Pampaloni, and M. Tedesco, "Microwave emission from dry snow: A comparison of experimental and model result," *IEEE Trans. Geosci. Remote Sens.*, vol. 39, no. 12, pp. 2649–2656, Dec. 2001.

[4] M. Tedesco, E. J. Kim, D. Cline, T. Graf, T. Koike, J. Hardy, R. Armstrong, and M. Brodzik, "Comparison of local-scale measured and modelled brightness temperatures and snow parameters from the Cold Land Processes Experiment 2003 by a dense medium theory model," *Hydrol. Processes*, Dec. 2005. To be published.

[5] A. T. C. Chang, J. L. Foster, and D. K Hall, "Nimbus 7 SMMR derived global snow cover patterns," *Ann. Glaciol.*, vol. 9, no. 39, pp. 39–44, 1989.

[6] J. Foster, A. Chang, and D. Hall, "Comparison of snow mass estimates from a prototype passive microwave snow algorithm, a revised algorithm and a snow depth climatology," *Remote Sens. Environ.*, vol. 62, no. 2, pp. 132–142, Nov. 1997.

[7] M. Tedesco, J. Pulliainen, P. Pampaloni, and M. Hallikainen, "Artificial neural network based techniques for the retrieval of SWE and snow depth from SSM/I data," *Remote Sens. Environ.*, vol. 90, no. 1, pp. 76–85, Mar. 2004.

[8] Y. Q. Jin, *Electromagnetic Scattering Modelling for Quantitative Remote Sensing*. Singapore: World Scientific, 1993.

[9] L. Tsang, J. A. Kong, and R. T. Shin, *Theory of Microwave Remote Sensing*. Hoboken, NJ: Wiley-Interscience, 1985.

[10] A. England and R. D. Roo, *CLPX-Ground: University of Michigan Ground-Based Microwave Radiometer*. Boulder, CO: Nat. Snow and Ice Data Center, Digital Media, 2004.

[11] A. Cagnati, A. Crepaz, G. Macelloni, P. Pampaloni, R. Ranzi, M. Tedesco, M. Tomirotti, and M. Valt, "Study of the snow melting–refreezing cycle using multi-sensor-data and snow modelling," *J. Glaciol.*, vol. 50, no. 170, pp. 419–126, Jun. 2005.

[12] M. Tedesco, "Microwave remote sensing of snow," Ph.D. dissertation, Inst. Appl. Phys. "Carrara," Italian Nat. Res. Council, IFAC—CNR, Microwave Remote Sensing Group, Florence, Italy, Nov. 2003.

[13] M. Tedesco, E. J. Kim, R. de Roo, A. W. England, H. Gu, H. Pham, and D. Boprie, "Forward modeling of measured CLPX 2003 snow brightness temperatures during melting/refreezing cycles by a multi-layer model based on dense medium radiative transfer theory," in *Proc. IEEE AP-S Int. Symp., USNC/URSI Nat. Radio Sci. Meeting*, Washington, DC, Jul. 3–8, 2005.

[14] S. E. Shih, K. H. Ding, J. A. Kong, R. E. Davis, J. P. Hardy, and A. Jordan, "Modeling of millimeter wave backscatter of time-varying snow cover based on dense medium radiative transfer theory and SNtherm," *J. Electromagn. Waves Appl.*, vol. 11, no. 9, pp. 1289–1298, 1997.

[15] J. Hardy, J. Pomeroy, T. Link, D. Marks, D. Cline, K. Elder, and R. Davis, *Snow Measurements at the CLPX Local Scale Observation Site (LSOS)*, M. Parsons and M. J. Brodzik, Eds. Boulder, CO: Nat. Snow and Ice Data Center. Digital Media, 2003. In situ data.

[16] G. Hufford, "A model for the complex permittivity of ice at frequencies below 1 THz," *Int. J. Infrared Millim. Waves*, vol. 12, no. 7, pp. 677–682, Jul. 1991.

[17] C. F. Bohren and D. R. Huffman, *Absorption and Scattering of Light by Small Particles*. New York: Wiley, 1983.

[18] J. R. Wang, P. E. O'Neill, T. J. Jackson, and E. T. Engman, "Multifrequency measurements of the effects of soil moisture, soil texture and surface roughness," *IEEE Trans. Geosci. Remote Sens.*, vol. GRS-21, no. 1, pp. 4–51, Jan. 1983.

[19] C. Mätzler, "Applications of SMOS over terrestrial ice and snow," in *Proc. 3rd SMOS Workshop*, Oberpfaffenhofen, Germany, Dec. 10–12, 2001.

[20] H. Wang, A. N. Arslan, J. Pulliainen, and M. Hallikainen, "Microwave emission model for wet snow by using radiative transfer and strong fluctuation theory," *J. Electromagn. Waves Appl.*, vol. 15, no. 1, pp. 1–148, 2001.

Marco Tedesco (S'01–M'05) received the laurea degree in electronic engineering from the University of Napoli "Federico II," Napoli, Italy, in November 1999, and the Ph.D. degree from the Institute of Applied Physics "Carrara," Firenze, Italy, in February 2004.

He was a Visiting Scientist with the Chinese Academy of Science, Beijing, China, with Fudan University, Shanghai, China, and with the Space Laboratory, Helsinki University of Technology. He also collaborated with the Group of Interaction between Electromagnetic Fields and Matter, Institute of Research on Electromagnetic Waves, publishing several peer-reviewed papers on microwave measurement techniques. In October 2003, he joined the Hydrospheric and Biospheric Sciences Laboratory, NASA's Goddard Space Flight Center, Goddard Earth Science and Technology Center, University of Maryland, Baltimore County. His research interests include remote sensing of snow, ice and soil; data fusion and assimilation; spatial behavior of geophysical parameters and remote sensing data; retrieval of snow impurities from optical measurements; merging hydrological and electromagnetic models; and measurement of dielectric properties of natural media. He serves as a Reviewer for several journals. He is also a Guest Editor of the Special Issue *Remote Sensing of the Cryosphere* on the journal *Remote Sensing of Environment*.

Dr. Tedesco received the NASA Outstanding PostDoc/Research Associate Peer Award in August 2005 and the Young Scientist URSI Award in October 2005. He is a member of the IEEE Geoscience and Remote Sensing Society (GRSS), American Geophysical Union Society, Technical Committee of Frequency Allocation in Remote Sensing of the GRSS, and National Geographic Society.

Edward J. Kim (S'86–M'86–SM'05) received the S.B. and S.M. degrees in electrical engineering from the Massachusetts Institute of Technology, Cambridge, and the Ph.D. degree from the University of Michigan, Ann Arbor, in 1998.

Since 1992, he has been involved in various Earth remote sensing projects. In 1997, he was selected for a National Research Council Research Associateship. Since 1999, he has been with the Hydrospheric and Biospheric Sciences Laboratory, NASA's Goddard Space Flight Center, Greenbelt, MD, developing and applying remote sensing techniques, particularly related to the terrestrial water cycle. Recently, he spearheaded efforts at Goddard to support a satellite proposal from the Cold Land Processes community. His interests include the modeling of snow, ice, soil, and vegetation; radiative transfer theory; and the development of new observational tools. He is Principal Investigator for several NASA airborne and ground-based radiometers. He serves the U.S. NPOESS program as Senior Instrument Scientist for the ATMS microwave atmospheric sounder, and as a member of the Microwave Operational Algorithm Team. Recently, he was selected by ESA as a Principal Investigator on the SMOS Validation and Retrieval Team.

Dr. Kim was awarded second prize in the 1998 International Geoscience and Remote Sensing Symposium student paper competition.

Anthony W. England (M'87–SM'89–F'95) received the Ph.D. degree in geophysics from the Massachusetts Institute of Technology, Cambridge, in 1970.

He was a Research Geophysicist and Deputy Chief with the Office of Geochemistry and Geophysics, U.S. Geological Survey, from 1972 to 1979. He was a Scientist–Astronaut during two periods with NASA, where he served as Mission Scientist for Apollo's 13 and 16, Mission Specialist on the Spacelab 2 flight in 1985, and Space Station Program Scientist in 1986–1987. He was a Visiting Adjunct Professor with Rice University in 1987. He has been Co-Investigator for the Apollo 17 surface electrical properties experiment and Co-Investigator on Shuttle Imaging Radar-A and -C experiments. In 1988, he joined the University of Michigan, Ann Arbor, where he is currently a Professor of electrical engineering and computer science, a Professor of atmospheric, oceanic, and space sciences, and an Associate Dean for Academic Affairs in the College of Engineering, University of Michigan. His research has included scattering theory applied to the microwave brightness of the Earth and planets, and the development and use of ice-sounding radar for the study of glaciers in Alaska and Antarctica. His current research focuses upon developing and calibrating land-surface process/radiobrightness models of land–atmosphere energy and moisture fluxes for the Arctic, and upon developing new radiometer technologies. He has been an Associate Editor for the *Journal of Geophysical Research*.

Dr. England is a member of the American Geophysical Union. He is a member of the Administrative Committee of IEEE's Geoscience and Remote Sensing Society, a member of the National Research Council's Space Studies Board, and the Chair of several federal committees concerned with science and technology policy.

Roger D. De Roo (S'88–M'96) received the B.S. degree in letters and engineering from Calvin College, Grand Rapids, MI, in 1986 and the B.S.E., M.S.E., and Ph.D. degrees from the University of Michigan, Ann Arbor, in 1986, 1989, and 1996, respectively, all in electrical engineering. His thesis was on the modeling and measurement of bistatic scattering of electromagnetic waves from rough dielectric surfaces.

From 1996 to 2000, he was a Research Fellow with the Radiation Laboratory, Department of Electrical Engineering and Computer Science, University of Michigan, investigating the modeling and simulation of millimeter-wave backscattering phenomenology of terrain at near grazing incidence. He is currently an Assistant Research Scientist with the Atmospheric, Oceanic, and Space Sciences Department, University of Michigan. His current research interests include digital correlating radiometer technology development and inversion of geophysical parameters such as soil moisture, snow wetness, and vegetation parameters from radar and radiometric signatures of terrain. He has supervised the fabrication of numerous dual-polarization microcontroller-based microwave radiometers.

Janet P. Hardy since joining the Cold Regions Research and Engineering Laboratory, Hanover, NH, in 1991, has conducted research in the field of snow hydrology, snowpack physics, and especially the understanding of fluxes, storage, and transformations of energy and water in complex forested environments. Her findings are integrated into existing models to improve representations of these processes in the terrestrial cryosphere.